J. Plasma Phys. (2024), *vol*. 90, 905900102 © The Author(s), 2024.
Published by Cambridge University Press
doi:10.1017/S0022377822000794

Improved numerical simulation model for nuclear reaction rate calculations in high-speed plasma collisions

Bo Zeng [1], Zijia Zhao [1,†], Xiaohu Yang [1,2,†], Shaowu Yang [1] and Yanyun Ma [2,3,†]

[1]Department of Physics, National University of Defense Technology, Changsha 410073, PR China

[2]Collaborative Innovation Centre of IFSA, Shanghai Jiao Tong University, Shanghai 200240, PR China

[3]College of Advanced Interdisciplinary Studies, National University of Defense Technology, Changsha 410073, PR China

(Received 13 May 2022; revised 18 August 2022; accepted 18 August 2022)

Beam–target reactions in fusion plasmas play an important role in both magnetic confinement fusion and inertial confinement fusion in the condition of low-density plasmas with high-velocity interactions. The traditional method for calculating beam–target reaction rate neglects the transport process of incident particles in inhomogeneous plasmas, leading to errors providing that the temperature and density in the transport path of incident particles vary obviously. An improved method considering the transport process is proposed in this paper to eliminate the deficiencies. Then the method is employed in high-speed plasma collision studies. When the initial plasma density and temperature are set to 0.5 g cm^{-3} and 100 eV, it is found that the beam–target reaction rate calculated by the traditional method is almost identical to that by our method if the collision velocity is less than 600 km s^{-1}. However, the traditional method is not suitable for study as the collision velocity gets higher, inducing obvious differences, which can reach 70 % at 1000 km s^{-1}. The improved method will make large corrections to evaluate the importance of the non-negligible beam–target reaction for inertial confinement fusion schemes with large implosion velocity such as double-cone ignition and impact ignition, in which the high-speed plasmas collide with each other to realize plasma ignition.

Key words: fusion plasma, intense particle beams

1. Introduction

Controlled fusion is one of the most promising methods for solving the energy crisis in the future (Wesson & Campbell 2011). The reaction can be divided into three categories according to the velocity distribution of reactants: thermonuclear reaction, beam–target reaction and beam–beam reaction (Dolan 2013). The thermonuclear reaction is caused by high-temperature plasmas with Maxwellian distributions, for which the reactivity can be

† Email addresses for correspondence: zhaozijia@nudt.edu.cn, xhyang@nudt.edu.cn, yanyunma@126.com

https://doi.org/10.1017/S0022377822000794 Published online by Cambridge University Press

calculated by (Atzeni & Meyer-ter Vehn 2004)

$$\langle \sigma v \rangle = \left(\frac{\beta}{\pi}\right)^{3/2} \int \mathrm{d}v v^3 \sigma(v) \mathrm{e}^{-\beta v^2}, \tag{1.1}$$

where v is the relative velocity, $\beta = (\beta_1 + \beta_2)/(\beta_1\beta_2)$, with $\beta_i = m_i/(2kT_i)$, and $\sigma(v)$ is the nuclear reaction cross-section depending on v. The thermonuclear reactivity only depends on temperature.

High-energy incident particles in plasmas can be slowed down by Coulomb scattering, nuclear scattering and other interactions. The particles would undergo fusion reaction with surrounding plasmas before they lose all of the kinetic energy and reach local thermodynamic equilibrium. The fusion reaction during the slowing-down process is called the beam–target reaction. The beam–target reaction is caused by incident particles with a monoenergetic distribution and target plasmas with a Maxwellian distribution. The reactivity can be expressed by (Dolan 2013)

$$\langle \sigma v \rangle_b = \sqrt{\frac{\beta_2}{\pi}} \frac{1}{v_b} \int \mathrm{d}v v^2 \sigma(v) [\exp(-\beta_2 (v - v_b)^2) - \exp(-\beta_2 (v + v_b)^2)], \tag{1.2}$$

where v_b is the velocity of the particles with monoenergetic distribution. The beam–beam reaction is caused by two plasmas both with monoenergetic distributions, which is usually too small and can be ignored.

The thermonuclear reaction is the most important one in both magnetic confinement fusion (Ongena *et al.* 2016) and inertial confinement fusion (ICF) (Betti & Hurricane 2016). The beam–target reaction is widely studied in tokamak neutral beam injection (Cordey, Keilhacker & Watkins 1987; Wilhelmsson 1987; Dawson, Furth & Tenney 1971; Hendel *et al.* 1986). The most general scenario is the injection of deuterium and tritium beams into a DT plasma. It is found that the thermonuclear reaction is dominant in high-density ($> 10^{20}\,\mathrm{m}^{-3}$) plasmas, such as conventional reactor operation; the beam–target reaction becomes dominant at moderate densities ($2\text{–}4 \times 10^{19}\,\mathrm{m}^{-3}$), this regime often being called the two-component torus (Wilhelmsson 1987). At low densities ($< 2 \times 10^{19}\,\mathrm{m}^{-3}$), it is necessary to take the beam–beam reaction into account. When the neutral beams are both co- and counter-injected with roughly equal magnitude, this regime is often referred to as the colliding-beam torus (Cordey & Core 1975; Jassby 1976). Experimental results in JET also show that the beam–target reaction is comparable with the thermonuclear reaction in neutral beam injection (Jarvis 1999).

The beam–target reaction also plays an important role in intense laser–plasma interactions. For example, a beam–target neutron source is widely studied to produce neutrons with high energy and low divergence angle (Zweiback *et al.* 2000; Lu *et al.* 2009; Willingale *et al.* 2011). Intense laser beams are focused onto a target and accelerate particles to high energy by various acceleration mechanisms such as target neutral sheath acceleration (Wilks *et al.* 2001) and breakout afterburner acceleration (Henig *et al.* 2009). Then the high-energy particles bombard the fuel target and produce neutrons by means of the beam–target reaction. Roth *et al.* (2013) accelerated deuterium ions using breakout afterburner acceleration to bombard a Be target and obtained a neutron yield of $10^{10}\,\mathrm{sr}^{-1}$. The energy of generated neutrons is up to 150 MeV, which is the highest energy obtained using a beam–target neutron source at present.

As for fusion ignition schemes research, He *et al.* (2015) proposed a spherical shell target scheme where a CD_2 layer was set outside to react with high-energy ions travelling across the cavity centre through beam–target reaction to deposit more energy. Finally, the energy

https://doi.org/10.1017/S0022377822000794 Published online by Cambridge University Press

conversion efficiency from laser to target can reach as high as 71 %. The beam–target reaction and thermonuclear reaction dominate in different stages and the peak neutron yield is 10^3 and $10^5\,\mathrm{J}^{-1}$, respectively. Zhang *et al.* (2017) observed anomalous neutron yield in indirect-drive ICF, and they attributed it to electrostatic shock wave collisions. Some of the deuterium particles are accelerated to high energy by the electrostatic shock wave and react with centre plasmas by means of the beam–target reaction (Zhang *et al.* 2017; Shan *et al.* 2018). Other research such as that concerning laser-driven plasma collider (Fu *et al.* 2015) also takes the beam–target reaction into account.

Generally speaking, the beam–target reaction is more likely to be encountered in magnetic confinement fusion because of the relatively high beam energy and low density. But in ICF research, when the implosion velocity is large enough, a large beam–target reaction may be induced. It is necessary to employ a precise calculation method in order to evaluate quantitatively the importance of the beam–target reaction rate in fusion. However, the traditional method (Yue *et al.* 1993; Perkins *et al.* 2000; He *et al.* 2015; Zhang *et al.* 2017; Shan *et al.* 2018) ignores the transport process and may introduce large errors when the temperature and density along the transport path of incident plasmas vary obviously. An improved method is proposed in this paper, in which we take the transport process into account to eliminate the errors.

The paper is organized as follows. In § 2 the traditional method and its deficiencies are introduced. An improved method is proposed to ameliorate the deficiencies. In § 3 a high-speed plasma collisions model is established and the two methods are applied to the model at the same time to display the differences. In § 4 calculation results are described and some conclusions are drawn. Section 5 is a brief summary. The improved method will be beneficial to ICF schemes with large implosion velocity like double-cone ignition (Zhang *et al.* 2020) and impact ignition (Murakami *et al.* 2014, 2005), in which high-speed plasmas collide with each other and realize ignition.

2. Algorithm for beam–target reaction rate calculation

Here we will take the DD reaction as an example, and assume that: (1) the deuterium ion beam undergoes no angular scattering during its transport (Perkins *et al.* 2000) and (2) for the incident plasmas, the velocity distribution can be regarded as a monoenergetic distribution and for the target plasmas can be regarded as a Maxwellian distribution. As regards target plasmas, the velocity is always too low and can be ignored. In this work, the velocities are set to 300, 600 and 1000 km s^{-1}. For deuterium particles, the corresponding kinetic energies are 0.94, 3.76 and 10.45 keV, respectively, which is around three times higher than the thermal energy (i.e. temperature) as displayed in table 2. As regards incident plasmas, the velocity is close to the initial setting value, which makes the kinetic energies much larger than the thermal energies. Thus, ignoring the thermal energy of incident plasmas would not lead to large errors.

According to (1.1) and (1.2), the thermonuclear reactivity only depends on target temperature, while the beam–target reactivity depends on both target temperature and beam energy. Figure 1 shows the thermonuclear reactivity and beam–target reactivity for the DD reaction with different beam energies and target temperatures. It is seen that the beam–target reactivity is comparable to the thermonuclear one for beam plasma energies from 0 to 10 keV and target plasma temperatures from 1 to 4 keV. The beam–target reactivity and thermonuclear reactivity both increase as the beam energy or the target temperature increase. However, the ratio of beam–target reactivity to thermonuclear reactivity increases as the beam plasma energy increases, while it decreases as the target plasma temperature increases. Other work has more detailed descriptions for conditions with larger beam energy and target temperature (Niikura, Nagami & Horiike 1988).

https://doi.org/10.1017/S0022377822000794 Published online by Cambridge University Press

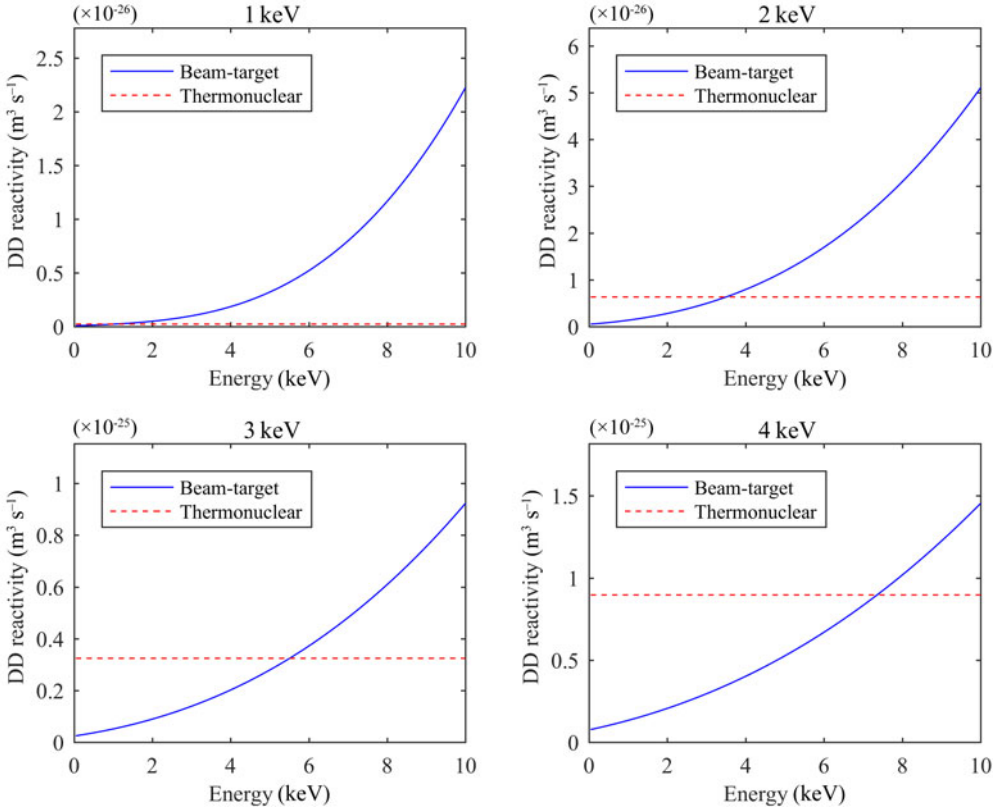

FIGURE 1. Comparison of beam–target reactivity and thermonuclear reactivity for the DD reaction with different target plasma temperatures and beam plasma energies.

High-speed beam ions occur in the beam–target reaction with surrounding plasmas while slowing down, and the neutrons produced during the whole slowing-down process have to be taken into account. When a deuterium ion with energy E propagates in the plasma, the energy loss during a given time dt is

$$\mathrm{d}E_i = -\varepsilon\,\mathrm{d}r = -\varepsilon v_i\,\mathrm{d}t, \tag{2.1}$$

where ε is the stopping power. It is a function of beam energy, target density and target temperature.

The number of beam–target reactions caused in this process can be expressed by

$$\mathrm{d}N_n = n_D\langle\sigma v\rangle_b\,\mathrm{d}t, \tag{2.2}$$

where $\langle\sigma v\rangle_b$ is the beam–target reactivity obtained by (1.2). According to (2.1) and (2.2), the total number of beam–target reactions caused by the beam ions is

$$N_n = \int_0^{E_i} n_D\langle\sigma v\rangle_b \frac{\mathrm{d}E}{v_i\varepsilon}. \tag{2.3}$$

Assuming the incident ion velocity distribution is f_i, then the total reaction caused by incident ions can be calculated (He *et al.* 2015; Zhang *et al.* 2017; Shan *et al.* 2018;

https://doi.org/10.1017/S0022377822000794 Published online by Cambridge University Press

Perkins *et al.* 2000):

$$N_{\mathrm{tot},b} = \int_0^{\infty} f_i \,\mathrm{d}E_i \int_0^{E_i} n_D \langle \sigma v \rangle_b \frac{\mathrm{d}E}{v_i \varepsilon} \Delta V. \tag{2.4}$$

For the thermonuclear reaction,

$$N_{\mathrm{tot},t} = \frac{1}{2} n_D^2 \langle \sigma v \rangle \Delta t \Delta V. \tag{2.5}$$

Equation (2.4) provides a convenient method to calculate the total beam–target reaction rate during the slowing-down process. The beam–target reaction rate and thermonuclear reaction rate can be estimated according to (2.4) and (2.5). In addition, some authors write $\langle \sigma v \rangle_b / v_i$ as σ in (2.4). That means the target plasma temperature is too low and can be ignored, i.e. cold target, and $\langle \sigma v \rangle_b$ is equal to σv_i in this case.

However, there is an obvious defect in (2.4). The stopping power ε is a function of beam plasma energy, target plasma temperature and density. The beam–target reactivity $\langle \sigma v \rangle_b$ is a function of beam energy and target temperature. Equation (2.4) only integrates the beam ion energy and considers the target plasma temperature and density as constant. But in reality, the temperature and density in the transport trace of incident particles may change much in inhomogeneous plasmas. If the range of incident particles is sufficiently smaller than the inhomogeneity length of the plasma, (2.4) is accurate. Otherwise, the equation may lead to large errors.

An example with one-dimensional simulation is shown in figure 2. A deuterium ion travels in the CD plasma system with a velocity of $1000\,\mathrm{km\,s^{-1}}$ (equal to the thermal velocity of a deuterium ion with 10 keV kinetic energy) from $x = 0$. The grid size is set to $1.3\,\mu\mathrm{m}$. The density and temperature are different in the two grids and the specific values are shown in figure 2(*a*). The results without transport process are obtained directly if we set $T = T_1$, $\rho = \rho_1$ during the entire integral path. While if we set $T = T_1$, $\rho = \rho_1$ when $x < l$ and $T = T_2$, $\rho = \rho_2$ when $x \geqslant l$, the results considering the transport process can be obtained, which are shown in figure 2(*b*). As shown in figure 2(*b*), the range of incident particles is around $2\,\mu\mathrm{m}$ in the initial grids, which is larger than the grid size. Thus, the temperature and density change obviously in the transport path and errors may appear. The results without transport are identical to those with transport when $x < 1.3\,\mu\mathrm{m}$, and the results with transport process deviate from the trend rapidly at $x = 1.3\,\mu\mathrm{m}$ due to the fact that the density and temperature vary much at this point. Finally, the total beam–target reactions for the cases without and with the influence of the transport process are 8.67×10^{-4} and 1.17×10^{-3}, respectively.

The integral value of (2.4) depends on the transport path. However, the density and temperature in the transport path are much different in different physical models. As a result, more detailed simulations should be employed to calculate the beam–target reaction rate accurately. An improved method to calculate the beam–target reaction rate in a specific physical model is proposed, as shown in figure 3.

Our proposed scheme is as follows:

Step 1. Using a radiation hydrodynamics program to simulate the physical process, and the density and ion temperature distribution in each grid could be obtained.

Step 2. For a time t_i, searching for the target plasma area. The velocity inside the target plasma area is relatively low and the density and temperature are relatively high. The division criterion depends on the specific physical model.

Step 3. According to the velocity, determining which grid can enter the target plasma area at a given time, i.e. incident plasma grid. For the time t_i, assuming all the particles

https://doi.org/10.1017/S0022377822000794 Published online by Cambridge University Press

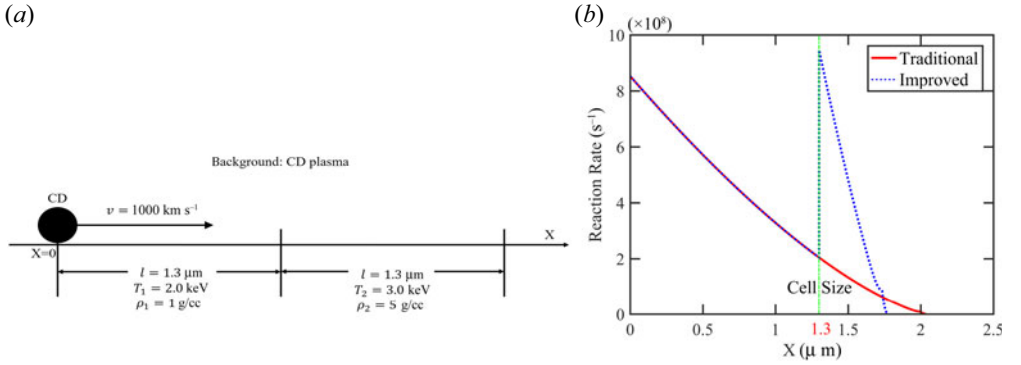

FIGURE 2. Diagram of one-dimensional simulation to show discrepancies in the traditional method. (*a*) A deuterium ion with a velocity of 1000 km s^{-1} travels in the CD plasma system. (*b*) The reaction rate for the cases with and without transport process.

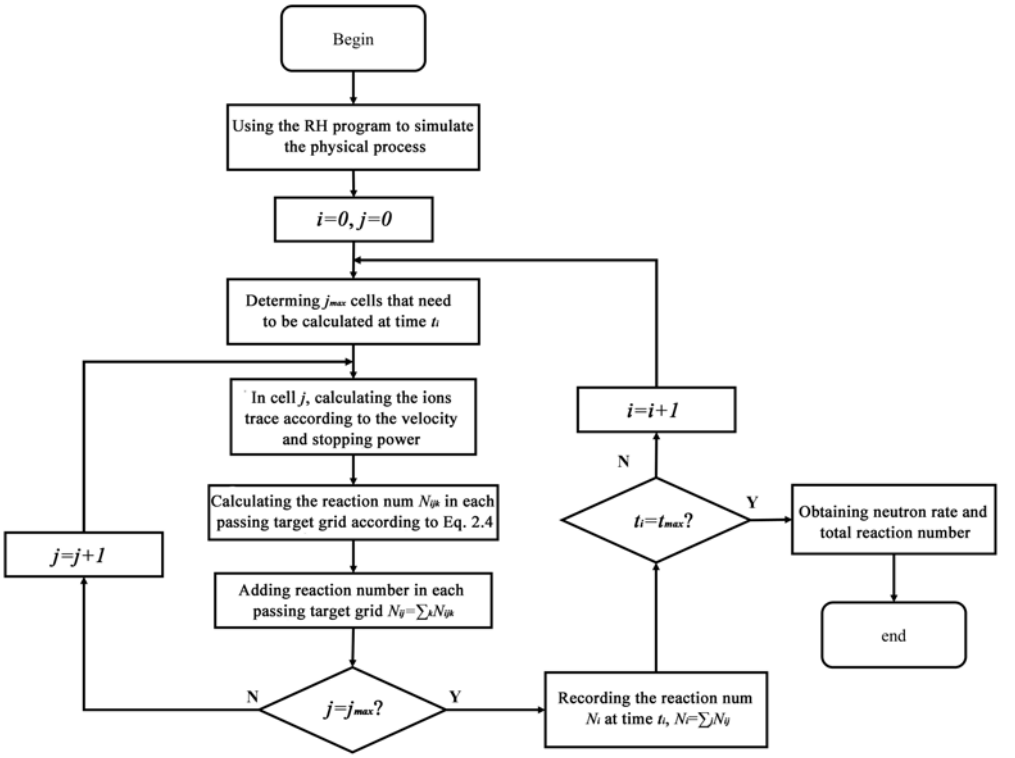

FIGURE 3. Flow chart of the improved beam–target reaction rate calculation algorithm.

in the incident plasma grids could enter other grids with a monoenergetic velocity distribution.

Step 4. Calculating the transport path for each incident grid. Then calculating the total reaction number. The incident plasma may pass through several grids. Since the temperature and density are quite different in different grids, the beam–target reaction rate in each target grid has to be calculated independently. Then they are added to get

https://doi.org/10.1017/S0022377822000794 Published online by Cambridge University Press

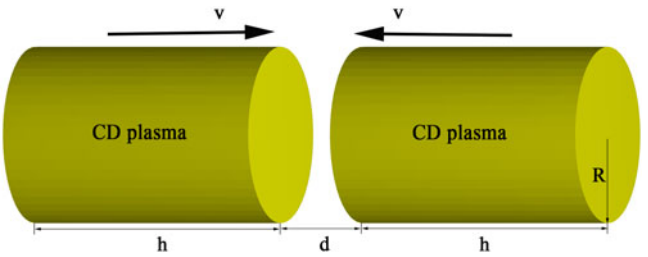

FIGURE 4. Diagram of the high-speed plasma collisions model.

the total beam–target reaction number. The calculation method is similar to (2.4) which calculates the beam–target reaction rate independently in each grid.

3. Simulation model

In order to see the importance of the beam–target reaction in high-speed plasma collisions, we consider two cylindrical CD plasmas with high-speed collisions, as shown in figure 4. The CD plasmas move towards each other with high velocity and collide head-on. Because of the high temperature and density in the collision area, a large thermonuclear reaction may occur in this region.

The radiation hydrodynamic program FLASH can meet the research needs (Fryxell *et al.* 2000). FLASH is an open-source program developed by the University of Chicago for more than 20 years. The program is widely used in the areas of high-energy-density physics and ICF research. The equation of state data are generated from the FEOS code (Young & Corey 1995; Faik, Tauschwitz & Iosilevskiy 2018) and the opacity data are calculated using the SNOP code (Eidmann 1994), which are both widely used data. In this paper, a two-dimensional cylindrical coordinate model is employed to simulate the collision process. Here we set $d = 0$ and $h = 0.3$ mm. The initial density of the high-speed plasma is set to $0.5\ \mathrm{g\,cm^{-3}}$ and the initial temperature is set to 100 eV. For comparison, the velocities are set to 300, 600 and $1000\ \mathrm{km\,s^{-1}}$, respectively. The radii of the CD plasma are set to 0.05, 0.10 and 0.15 mm, respectively. The grid size is set to $1.3\ \mu\mathrm{m}$.

Note that in laser-driven neutron source research, the PIC+MC code is widely used. But it is not suitable for our model. Because of numerical noise, the PIC method could only simulate cases of several hundred micrometres and several hundred femtoseconds. It is not suitable for investigating cases with large spatial scale and time scale. In these cases, a radiation hydrodynamic program should be applied.

The nuclear reaction cross-section data here are obtained from the ENDF database (Chadwick *et al.* 2011) and the stopping power data are from the classic model (Honrubia & Murakami 2015) given by

$$\frac{\mathrm{d}E}{\mathrm{d}x} = \sum_j \frac{2\pi q^2 q_i^2 m \ln(\Lambda_j)}{m_j E} n_j G(x_j), \tag{3.1}$$

where $\ln(\Lambda_j)$ is the Coulomb logarithm. The subscript j means different particles, including electron and deuterium particles. Also,

$$G(x) = \mathrm{erf}(x) - \frac{2}{\sqrt{\pi}} x\,\mathrm{e}^{-x^2} \quad \text{and} \quad x_j = \frac{v}{v_j} = \frac{v}{\sqrt{2\theta_j/m_j}}, \tag{3.2a,b}$$

https://doi.org/10.1017/S0022377822000794 Published online by Cambridge University Press

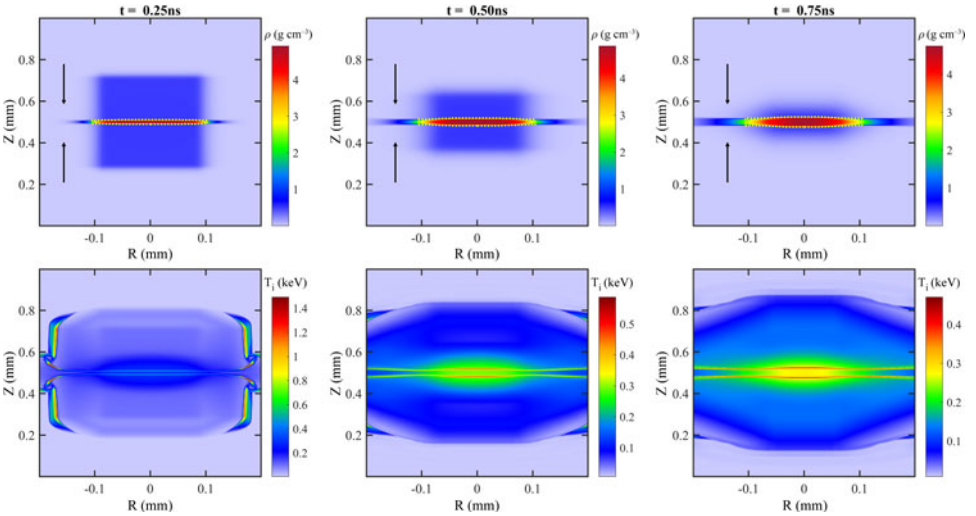

FIGURE 5. Density distribution and ion temperature distribution for the case of $v = 300\,\mathrm{km\,s^{-1}}$ and $R = 0.10\,\mathrm{mm}$. The dotted line is the division result of the collision area described in Step 2 in § 2.

where $\mathrm{erf}(x)$ is an error function given by

$$\mathrm{erf}(x) = \frac{2}{\sqrt{\pi}} \int_0^x \mathrm{e}^{-\eta^2}\,\mathrm{d}\eta. \tag{3.3}$$

Parameters m_j, q_j, v_j and θ_j are the mass, charge, average particle velocity and average temperature of particles j, respectively.

The temperature and density inside the collision area are relatively high and the velocity is relatively low. Thus, the collision area should be regarded as the target plasma area. The velocity outside the collision area is relatively large so that the velocity gradient is a good criterion for dividing the collision area.

4. Results and discussion

The density distribution and ion temperature distribution for the case of $v = 300\,\mathrm{km\,s^{-1}}$ and $R = 0.10\,\mathrm{mm}$ are shown in figure 5. The white dotted line in the density distribution in figure 5 is the collision area edge divided by velocity gradient. The division result shows that the collision area is of high density and relatively high ion temperature, so that it is an ideal place to induce the thermonuclear reaction.

It is seen that the CD plasmas are compressed after they collide at the centre area. The collision area is small with a peak density of around $5\,\mathrm{g\,cm^{-3}}$ at $t = 0.25\,\mathrm{ns}$, which is around 10 times larger than the initial density. At $t = 0.50\,\mathrm{ns}$, the collision area becomes larger and the peak density is almost the same as that at $t = 0.25\,\mathrm{ns}$. At $t = 0.75\,\mathrm{ns}$, the cylindrical plasmas outside the collision area are almost completely incident to the collision area. The range of collision area along the Z direction is around 0.1 mm. And the peak density is still around $5\,\mathrm{g\,cm^{-3}}$. The ion temperature has a similar evolution trend. At the beginning of the collision process, temperature may be very large in the cylinder outside edge because of the diffusion effect. At $t = 0.50\,\mathrm{ns}$, the high-temperature area becomes larger and the peak temperature in the collision area is around 0.3 keV, which is maintained to $t = 0.75\,\mathrm{ns}$.

https://doi.org/10.1017/S0022377822000794 Published online by Cambridge University Press

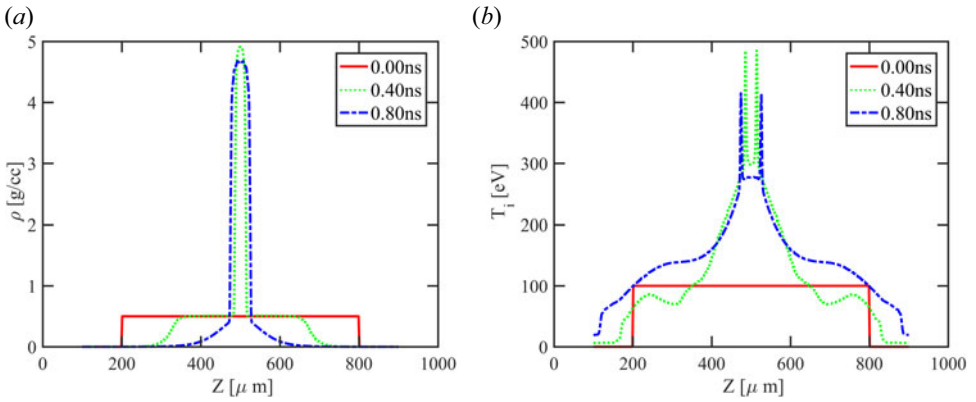

FIGURE 6. Density distribution (*a*) and ion temperature distribution (*b*) along the *Z* direction.

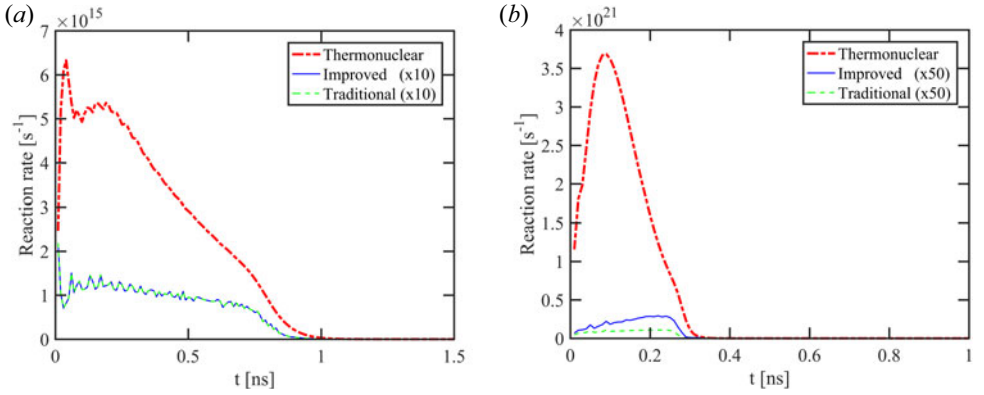

FIGURE 7. Reaction rate for the cases with (*a*) $v = 300\,\mathrm{km\,s^{-1}}$, $R = 0.10\,\mathrm{mm}$ and (*b*) $v = 1000\,\mathrm{km\,s^{-1}}$, $R = 0.10\,\mathrm{mm}$.

As we can see in figure 6, at $t = 0$ ns, the two cylindrical plasmas have not collided yet so that the temperature and density distributions are flat along the Z direction. At $t = 0.4$ ns, the density and temperature in the collision area reach the peak values of $5\,\mathrm{g\,cm^{-3}}$ and 0.3 keV, respectively. At $t = 0.8$ ns, the density and temperature decrease slightly and the collision region area becomes larger. It is seen that the temperature in the collision region edge is larger than that in the collision region. This can be attributed to the superposition effect of shock waves.

The reaction rates of thermonuclear reaction and beam–target reaction obtained by the traditional method and the improved method are shown in figure 7. It is seen that the thermonuclear reaction rate is much larger than the beam–target one. When $v = 300\,\mathrm{km\,s^{-1}}$, the peak thermonuclear reaction rate is around 30 times larger than the peak beam–target reaction rate. The results of the traditional method are almost identical to those of the improved method. However, when the velocity reaches $1000\,\mathrm{km\,s^{-1}}$, the peak thermonuclear reaction rate is hundreds of times larger than the peak beam–target reaction rate. The results of the traditional method are around two times lower than those of the improved method, indicating that the traditional method is not suitable for large-collision-velocity cases.

https://doi.org/10.1017/S0022377822000794 Published online by Cambridge University Press

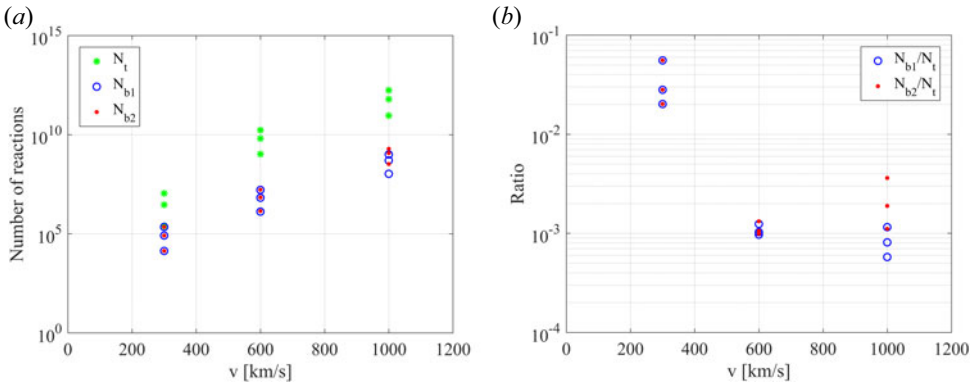

FIGURE 8. (*a*) Number of thermonuclear reactions and beam–target reactions by the traditional method and improved method. At the same velocity conditions, the three values of the same kind of reaction number from large to small correspond to $R = 0.05$, $R = 0.10$ and $R = 0.15$ mm, respectively. (*b*) Ratios of beam–target reaction to thermonuclear reaction by the traditional method and improved method. At the same velocity conditions, the three values of the same kind of ratios from large to small correspond to $R = 0.05$, $R = 0.10$ and $R = 0.15$ mm respectively.

The total neutron yield of thermonuclear reaction and beam–target reaction in each case is presented in table 1, which is also shown in figure 8. It is seen that the beam–target reaction numbers by the traditional method N_{b1} and by the improved method N_{b2} are almost the same at $v = 300\,\mathrm{km\,s^{-1}}$. When the velocity goes to $600\,\mathrm{km\,s^{-1}}$, slight differences appear. The two methods are different obviously at $v = 1000\,\mathrm{km\,s^{-1}}$. The discrepancy between the two methods can reach 70 %.

In addition, the following points can be made from table 1 and figure 8:

(i) Both the thermonuclear reaction number and beam–target reaction number increase as the velocity increases. However, the ratio of beam–target reaction to thermonuclear reaction decreases with an increase of the velocity in general.

(ii) The ratio of beam–target reaction by the improved method to thermonuclear reaction shows an anomalous increase at $v = 1000\,\mathrm{km\,s^{-1}}$. The reason is given below in terms of the results in table 2 and figure 9.

(iii) The beam–target reaction is more important (the ratio is larger) when the cylindrical radius is small. From the simulation result, because of the diffusion effect in the plasma cylinder outside surface, the collision region volume with high temperature increases faster than the volume of a cylinder as the cylindrical radius increases. Therefore, the thermonuclear reaction increases faster than the beam–target reaction as the cylindrical radius increases.

With the temperature in the collision area and the edge obtained from the simulation, according to (1.1) and (1.2), the reaction rate for different velocities and temperatures can be calculated, as shown in table 2. As seen in table 2, the ratio of beam–target reaction rate to thermonuclear reaction rate for $300\,\mathrm{km\,s^{-1}}$ is much larger than that for other velocity conditions. In the edge of the collision area, the ratios are 27.8, 4.08 and 3.10, respectively, when the velocities are 300, 600 and $1000\,\mathrm{km\,s^{-1}}$. The trend fits well the traditional method result in figure 8(*b*).

However, the improved method takes the transport process into consideration. When the velocity is high enough (e.g. $v = 1000\,\mathrm{km\,s^{-1}}$), the incident particles from the collision area edge may reach the collision centre, so that the ratios should be modified to 27.8, 4.08

https://doi.org/10.1017/S0022377822000794 Published online by Cambridge University Press

https://doi.org/10.1017/S0022377822000794 Published online by Cambridge University Press

Case	v (km s^{-1})	R (mm)	N_t	N_{b1}	N_{b1}/N_t (%)	N_{b2}	N_{b2}/N_t (%)	N_{b1}/N_{b2} (%)
1	300	0.05	2.44×10^5	1.36×10^4	5.56	1.36×10^4	5.56	100.00
2	300	0.1	2.90×10^6	8.14×10^4	2.81	8.14×10^4	2.81	100.00
3	300	0.15	1.09×10^7	2.21×10^5	2.02	2.21×10^5	2.02	100.00
4	600	0.05	1.05×10^9	1.30×10^6	0.12	1.39×10^6	0.13	94.09
5	600	0.1	6.38×10^9	6.56×10^6	0.10	6.76×10^6	0.11	97.05
6	600	0.15	1.69×10^{10}	1.64×10^7	0.10	1.67×10^7	0.10	98.15
7	1000	0.05	9.13×10^{10}	1.06×10^8	0.12	3.3×10^8	0.36	31.92
8	1000	0.1	6.16×10^{11}	4.99×10^8	0.08	1.16×10^9	0.19	42.87
9	1000	0.15	1.74×10^{12}	1.00×10^9	0.06	1.94×10^9	0.11	51.84

TABLE 1. Simulation result of various neutron yields. Here v is the velocity, R is the radius of the cylinder, N_t is the number of thermonuclear reactions, N_{b1} is the number of beam–target reactions by the traditional method and N_{b2} is the number of beam–target reactions by the improved method.

Case	v (km s^{-1})	$T_{i,e}$ (keV)	$n_{b,e}/n_{t,e}$	$T_{i,c}$ (keV)	$n_{b,c}/n_{t,c}$
1	300	0.5	27.80	0.3	5921.65
2	600	1.2	4.08	0.8	14.75
3	1000	3.0	3.10	2.5	4.79

TABLE 2. Simulation result of temperature for different conditions. Here $T_{i,e}$ is the ion temperature in the edge, $T_{i,c}$ is the ion temperature in the collision area, where the temperature data are from the simulation result directly, $n_{b,e}$ is the beam–target reaction rate in the collision area edge, $n_{b,c}$ is the beam–target reaction rate in the collision centre according to (1.2) and $n_{t,e}$ and $n_{t,c}$ are thermonuclear reaction rate in the collision area edge and collision centre, respectively.

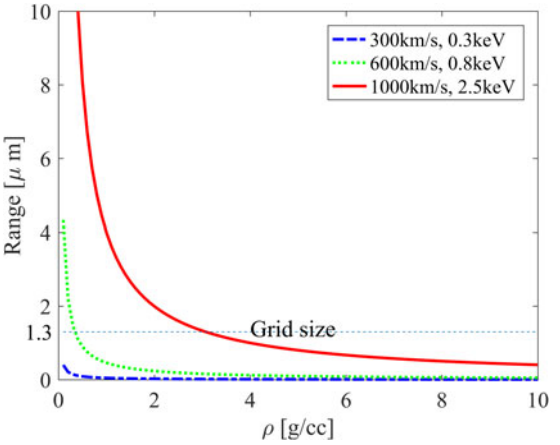

FIGURE 9. Range of incident particles for different beam velocity conditions in the collision area. Corresponding ion temperature for each velocity can be obtained from the simulation result as shown in table 2.

and 4.79, respectively. These ratios could explain why the ratio of the beam–target reaction by the improved method to the thermonuclear reaction shows an anomalous increase at $v = 1000\,\mathrm{km\,s^{-1}}$.

To prove this statement, the range of incident particles is shown in figure 9. Figure 9 is a rough estimate to the range of incident particles. It is seen that it is hard for the incident particle to leave its initial grid when the velocity is low. When the velocity reaches $1000\,\mathrm{km\,s^{-1}}$, the range of the incident particles is close to the grid size (1.3 μm) at a density of near $4\,\mathrm{g\,cm^{-3}}$ so that the particles may leave their initial grid and travel to neighbouring grids.

5. Summary

An improved method taking the incident particle transport process into account is proposed to calculate the beam–target reaction rate accurately. The method is applied to study high-speed plasma collisions. When the initial density and temperature are set to $0.5\,\mathrm{g\,cm^{-3}}$ and 100 eV, it is found that the results of the traditional method are close to those of the improved method if the collision velocity is less than $600\,\mathrm{km\,s^{-1}}$. However, large differences appear for the case with higher collision velocity. The differences

https://doi.org/10.1017/S0022377822000794 Published online by Cambridge University Press

between the two methods can reach 70 % at 1000 km s^{-1}. That is, the improved method can lead to much more accurate results for high-velocity conditions.

The thermonuclear reaction and beam–target reaction both increase much as the collision velocity increases. The ratio of beam–target reaction to thermonuclear reaction decreases with increasing collision velocity. When the collision velocity is high enough (e.g. 1000 km s^{-1}), because of plasma transport, the ratio of beam–target reaction to thermonuclear reaction may increase a little anomalously.

The improved method will make large corrections to evaluate the importance of the non-negligible beam–target reaction for ICF schemes with large implosion velocity, such as the double-cone ignition scheme and impact ignition scheme.

Acknowledgements

We would like to thank X. Jiang for beneficial discussions.

Editor Luís O. Silva thanks the referees for their advice in evaluating this article.

Funding

This work was supported by the Strategic Priority Research Program of Chinese Academy of Science (grant no. XDA25050200), the National Natural Science Foundation of China (grant nos. 12175309, 11775305, 11975308 and 12005297), the fund of Science Challenge Project (no. TZ2018001) and the State Key Laboratory of Laser Interaction with Matter (no. SKLLIM1908). X.H.Y. also acknowledges the financial support from Fund for NUDT Young Innovator Awards (no. 20180104).

Declaration of interests

The authors report no conflict of interest.

Author contributions

B.Z. and Z.Z. derived the theory and proposed the improved method. Results were prepared by S.Y. X.Y. and Y.M. contributed to data analysis. The article was written by B.Z.

Data availability

The data that support the findings of this study are available from the corresponding author upon reasonable request.

REFERENCES

Atzeni, S. & Meyer-ter Vehn, J. 2004 *The Physics of Inertial Fusion: Beam Plasma Interaction, Hydrodynamics, Hot Dense Matte*. Oxford University Press.

Betti, R. & Hurricane, O.A. 2016 Inertial-confinement fusion with lasers. *Nat. Phys*. **12** (5), 435–448.

Chadwick, M.B., Herman, M., Obložinský, P., Dunn, M.E., Danon, Y., Kahler, A.C., Smith, D.L., Pritychenko, B., Arbanas, G., Arcilla, R., *et al.* 2011 Endf/b-vii.1 nuclear data for science and technology: cross sections, covariances, fission product yields and decay data. *Nucl. Data Sheets* **112** (12), 2887–2996.

Cordey, J.G. & Core, W.G.F. 1975 The three-component toroidal reactor. *Nucl. Fusion* **15** (4), 710–712.

Cordey, J.G., Keilhacker, M. & Watkins, M.L. 1987 Prospects for alpha particle heating in jet in the hot ion regime. *Phys. Scr*. **T16**, 127–132.

Dawson, J., Furth, H. & Tenney, F. 1971 Production of thermonuclear power by non-maxwellian ions in a closed magnetic field configuration. *Phys. Rev. Lett*. **26**, 1156–1160.

Dolan, T.J. 2013 *Fusion Research: Principles*. Elsevier.

https://doi.org/10.1017/S0022377822000794 Published online by Cambridge University Press

EIDMANN, K. 1994 Radiation transport and atomic physics modeling in high-energy-density laser-produced plasmas. *Laser Part. Beams* **12**, 223–244.

FAIK, S., TAUSCHWITZ, A. & IOSILEVSKIY, I. 2018 The equation of state package feos for high energy density matter. *Comput. Phys. Commun*. **227**, 117–125.

FRYXELL, B., OLSON, K., RICKER, P., TIMMES, F.X., ZINGALE, M., LAMB, D.Q., MACNEICE, P., ROSNER, R., TRURAN, J.W. & TUFO, H. 2000 FLASH: an adaptive mesh hydrodynamics code for modeling astrophysical thermonuclear flashes. *Astrophys. J. Suppl. Ser*. **131** (1), 273–334.

FU, C., BAO, J., CHEN, L., HE, J., HOU, L., LI, L., LI, Y., LI, Y., LIAO, G., RHEE, Y., *et al.* 2015 Laser-driven plasma collider for nuclear studies. *Sci. Bull*. **60** (13), 1211–1213.

HE, M.Q., CAI, H.B., ZHANG, H., DONG, Q.L., ZHOU, C.T., WU, S.Z., SHENG, Z.M., CAO, L.H., ZHENG, C.Y., WU, J.F., *et al.* 2015 A spherical shell target scheme for laser-driven neutron sources. *Phys. Plasmas* **22** (12), 123103.

HENDEL, H.W., ENGLAND, A.C., JASSBY, D.L., MIRIN, A.A. & NIESCHMIDT, E.B. 1986 Fusion-neutron production in the tftr with deuterium neutral-beam injection. *J. Fusion Energy* **5** (3), 231–244.

HENIG, A., KIEFER, D., MARKEY, K., GAUTIER, D.C., FLIPPO, K.A., LETZRING, S., JOHNSON, R.P., SHIMADA, T., YIN, L., ALBRIGHT, B.J., *et al.* 2009 Enhanced laser-driven ion acceleration in the relativistic transparency regime. *Phys. Rev. Lett*. **103**, 045002.

HONRUBIA, J.J. & MURAKAMI, M. 2015 Ion beam requirements for fast ignition of inertial fusion targets. *Phys. Plasmas* **22** (1), 012703.

JARVIS, O. 1999 Neutron measurement techniques for tokamak plasmas. *Plasma Phys. Control. Fusion* **36**, 209.

JASSBY, D.L. 1976 Reactor aspects of counterstreaming-ion tokamak plasmas. *Nucl. Fusion* **16** (1), 15–29.

LU, H.Y., LIU, J.S., WANG, C., WANG, W.T., ZHOU, Z.L., DENG, A.H., XIA, C.Q., XU, Y., LU, X.M., JIANG, Y.H., *et al.* 2009 Efficient fusion neutron generation from heteronuclear clusters in intense femtosecond laser fields. *Phys. Rev.* A **80** (5), 051201.

MURAKAMI, M., NAGATOMO, H., JOHZAKI, T., SAKAIYA, T., VELIKOVICH, A., KARASIK, M., GUS'KOV, S. & ZMITRENKO, N. 2014 Impact ignition as a track to laser fusion. *Nucl. Fusion* **54** (5), 054007.

MURAKAMI, M., NAGATOMO, H., SAKAIYA, T., AZECHI, H., FUJIOKA, S., SHIRAGA, H., NAKAI, M., SHIGEMORI, K., SAITO, H., OBENSCHAIN, S., *et al.* 2005 Towards realization of hyper-velocities for impact fast ignition. *Plasma Phys. Control. Fusion* **47** (12B), B815–B822.

NIIKURA, S., NAGAMI, M. & HORIIKE, H. 1988 Characteristics of fusion reaction rate and neutron yield in deuterium plasma. *Fusion Engng Des*. **6**, 181–191.

ONGENA, J., KOCH, R., WOLF, R. & ZOHM, H. 2016 Magnetic-confinement fusion. *Nat. Phys*. **12** (5), 398–410.

PERKINS, L.J., LOGAN, B.G., ROSEN, M.D., PERRY, M.D., DE LA RUBIA, T.D., GHONIEM, N.M., DITMIRE, T., SPRINGER, P.T. & WILKS, S.C. 2000 The investigation of high intensity laser driven micro neutron sources for fusion materials research at high fluence. *Nucl. Fusion* **40** (1), 1–19.

ROTH, M., JUNG, D., FALK, K., GULER, N., DEPPERT, O., DEVLIN, M., FAVALLI, A., FERNANDEZ, J., GAUTIER, D., GEISSEL, M., *et al.* 2013 Bright laser-driven neutron source based on the relativistic transparency of solids. *Phys. Rev. Lett*. **110** (4), 044802.

SHAN, L.Q, CAI, H.B, ZHANG, W.S, TANG, Q., ZHANG, F., SONG, Z.F, BI, B., GE, F.J, CHEN, J.B, LIU, D.X, *et al.* 2018 Experimental evidence of kinetic effects in indirect-drive inertial confinement fusion hohlraums. *Phys. Rev. Lett*. **120** (19), 195001.

WESSON, J. & CAMPBELL, D.J. 2011 *Tokamaks*. Oxford University Press.

WILHELMSSON, H. 1987 Evolution of burning fusion plasma density and alpha particle production in approaching ignition. *Phys. Scr*. **16**, 176–178.

WILKS, S.C., LANGDON, A.B., COWAN, T.E., ROTH, M., SINGH, M., HATCHETT, S., KEY, M.H., PENNINGTON, D., MACKINNON, A. & SNAVELY, R.A. 2001 Energetic proton generation in ultra-intense laser–solid interactions. *Phys. Plasmas* **8** (2), 542–549.

WILLINGALE, L., PETROV, G.M., MAKSIMCHUK, A., DAVIS, J., FREEMAN, R.R., JOGLEKAR, A.S., MATSUOKA, T., MURPHY, C.D., OVCHINNIKOV, V.M., THOMAS, A.G.R., *et al.* 2011

https://doi.org/10.1017/S0022377822000794 Published online by Cambridge University Press

Comparison of bulk and pitcher-catcher targets for laser-driven neutron production. *Phys. Plasmas* **18** (8), 083106.

YOUNG, D. & COREY, E. 1995 A new global equation of state model for hot, dense matter. *J. Appl. Phys*. **78**, 3748–3755.

YUE, Z.W., SHEN, Y.P., WANG, S.W. & KUANG, H.S. 1993 The effect of non-equilibrium relaxation process of high-speed nucleus in high temperature thermal equilibrium plasma on fusion reaction rate parameter. *J. Natl Univ. Defense Technol.* **15** (4), 38–42.

ZHANG, W.S., CAI, H.B., SHAN, L.Q., ZHANG, H.S., GU, Y.Q. & ZHU, S.P. 2017 Anomalous neutron yield in indirect-drive inertial-confinement-fusion due to the formation of collisionless shocks in the corona. *Nucl. Fusion* **57** (6), 066012.

ZHANG, J., WANG, W.-M., YANG, X., WU, D., MA, Y.-Y., JIAO, J., ZHANG, Z., WU, F., YUAN, X., LI, Y., *et al.* 2020 Double-cone ignition scheme for inertial confinement fusion. *Phil. Trans. R. Soc.* A **378**, 20200015.

ZWEIBACK, J., COWAN, T.E., SMITH, R.A., HARTLEY, J.H., HOWELL, R., STEINKE, C.A., HAYS, G., WHARTON, K.B., CRANE, J.K. & DITMIRE, T. 2000 Characterization of fusion burn time in exploding deuterium cluster plasmas. *Phys. Rev. Lett*. **85** (17), 3640–3643.

https://doi.org/10.1017/S0022377822000794 Published online by Cambridge University Press